Phys Chem Minerals (2015) 42:213–222
DOI 10.1007/s00269-014-0712-y

ORIGINAL PAPER

Elastic wave velocity of polycrystalline $Mj_{80}Py_{20}$ garnet to 21 GPa and 2,000 K

Zhaodong Liu · Tetsuo Irifune · Steeve Gréaux · Takeshi Arimoto · Toru Shinmei · Yuji Higo

Received: 19 May 2014 / Accepted: 25 September 2014 / Published online: 18 October 2014

Abstract The elastic wave velocities of polycrystalline $Mj_{80}Py_{20}$ garnet along the majorite–pyrope system have been measured at pressures up to 21 GPa and temperatures up to 2,000 K using ultrasonic interferometry in conjunction with in situ X-ray diffraction techniques in a Kawai-type multi-anvil apparatus. The elastic moduli of $Mj_{80}Py_{20}$ garnet and their pressure and temperature derivatives are determined by a two-dimensional linear fitting of the present experimental data, yielding: $K_S = 161.5$ (7) GPa, $\partial K_S/\partial P = 4.42$ (4), $\partial K_S/\partial T = -0.0154$ (2) GPa/K, $G = 86.2$ (2) GPa, $\partial G/\partial P = 1.28$ (1), $\partial G/\partial T = -0.0096$ (5) GPa/K. The present results together with those of the studies on the majorite–pyrope solid solutions suggest the pressure and temperature derivatives of elastic moduli are insensitive to the majorite content in the majorite–pyrope system. The velocity gradients of the majoritic garnets in the majorite–pyrope system are 3 ~ 6 times lower than those required to account for the high seismic velocity gradients observed in the mantle transition zone.

Keywords Garnet · Elastic wave velocity · Elastic moduli · Velocity gradients

Z. Liu (✉) · T. Irifune · S. Gréaux · T. Arimoto · T. Shinmei
Geodynamics Research Center, Ehime University, Matsuyama 790-8577, Japan
e-mail: zhaodong@sci.ehime-u.ac.jp

T. Irifune · S. Gréaux
Earth-Life Science Institute, Tokyo Institute of Technology, Tokyo 152-8550, Japan

Y. Higo
Japan Synchrotron Radiation Institute, Hyogo 678-5198, Japan

Introduction

Majoritic garnet is a major constituent mineral in the Earth's mantle transition zone depths of 410–660 km along with wadsleyite and ringwoodite (Ringwood and Major 1971; Akaogi and Akimoto 1977; Irifune and Ringwood 1987). It was firstly synthesized at high pressure by Ringwood and Major (Ringwood and Major 1971) and subsequently identified in Catherwood meteorites (Coleman 1977; Mao et al. 1982) and diamond inclusions in mantle-derived xenoliths (Moore and Gurney 1985; Meyer 1987). Petrological studies have demonstrated that majoritic garnet is the most abundant mineral in basaltic layers of subducted lithosphere in the mantle transition zone depths (Irifune et al. 1986; Irifune and Ringwood 1993; Hirose et al. 1999; Ono et al. 2001). Accordingly, the physical properties of majoritic garnet are indispensable for constraining the mineralogical models of the mantle transition zone.

Previous studies have demonstrated that the simplified system $Mg_4Si_4O_{12}$ (majorite)–$Mg_3Al_2Si_3O_{12}$ (pyrope) is the most relevant and dominant solid system in the mantle transition zone (Irifune and Ringwood 1987, 1993; Irifune et al. 1996; Gasparik 1990, 1992; Kubo and Akaogi 2000; Akaogi et al. 2002). However, the elastic properties of majoritic garnets along the majorite–pyrope system investigated by earlier Brillouin scattering (Bass and Kanzaki 1990; Yeganeh-Haeri et al. 1990; Pacalo and Weidner 1997; Sinogeikin et al. 1997, Sinogeikin and Bass 2002a, b) and ultrasonic interferometry (Rigden et al. 1994; Liu et al. 2000; Gwanmesia et al. 2006, 2009; Zou et al. 2012) were largely scattered; for example, the pressure derivatives of the elastic moduli ranged from 3.2 to 6.7 and 1.0 to 2.1 for K_S' and G', respectively. The high sound velocity gradients, characteristic of this region (Bass and Anderson 1984; Sinogeikin and Bass 2002a), may be caused by the

unusually high-pressure derivatives of the elastic moduli of the majoritic garnets in this solid system (Gwanmesia et al. 1998; Kavner et al. 2000; Liu et al. 2000). The discrepancies on the elastic properties of the majoritic garnets in this system have impeded to interpret the seismic velocity profile of the mantle transition zone.

In addition, these earlier studies were performed at ambient conditions (Bass and Kanzaki 1990; Yeganeh-Haeri et al. 1990; Pacalo and Weidner 1997; Sinogeikin et al. 1997; Gwanmesia et al. 2000), high pressures at room temperature (Sinogeikin and Bass 2002a; Liu et al. 2000) or high temperatures at room pressure (Sinogeikin and Bass 2002b). There have been virtually no experimental studies on elastic properties of majoritic garnets at high-pressure and high-temperature conditions of the mantle transition zone, where majoritic garnet is believed to be stable and abundant volumetrically. The development of state-of-the-art experimental techniques of ultrasonic interferometry in conjunction with synchrotron X-ray diffraction allows us to investigate sound velocities of minerals at pressure and temperature conditions of the Earth's deep interior (Li et al. 1996, 2001, 2004, Li and Liebermann 2007; Higo et al. 2008, 2009). Gwanmesia et al. (2009) measured the elastic parameters of $Mj_{40}Py_{60}$ and $Mj_{50}Py_{50}$ garnets up to 8 GPa and 1,000 K. More recently, Zou et al. (2012) reported the elastic wave velocity of pyrope to 19 GPa and 1,700 K. To date, however, the elastic wave velocity studies on the majorite–rich garnets have been very limited; only the exception is Irifune et al. (2008), which reported the elastic wave velocity of majorite with a pyrolite minus olivine composition under high-pressure and high-temperature conditions of the mantle transition zone region. The majoritic garnet sample used in this study, however, has a more complex chemical composition than the end-member majorite in the majorite–pyrope system, the results of which are applicable only to address the behaviors of majorite with a pyrolite composition.

Here we performed in situ X-ray diffraction and ultrasonic measurements on a majoritic garnet in the majorite–pyrope system at simultaneous high pressures and high temperatures in a Kawai-type multi-anvil apparatus. The elastic moduli and their pressure and temperature derivatives are determined from the current experimental data. The newly obtained results are compared with those from the previous studies on other majoritic garnets with various compositions along the majorite–pyrope system.

Experimental method

Synthetic polycrystalline $Mj_{80}Py_{20}$ garnet

The polycrystalline majoritic garnet was synthesized at 19 GPa and 1,700 °C for 2 h from a glass with composition of 95 mol % $MgSiO_3$ and 5 mol % Al_2O_3 [i.e., 80 mol % $Mg_4Si_4O_{12}$ (Mj) and 20 mol % $Mg_3Al_2Si_3O_{12}$ (Py)] using a Kaiwai-type multi-anvil apparatus (Orange-3000) at the Geodynamics Research Center, Ehime University, Japan. The hot-pressed specimen was well sintered, translucent, and cylindrical in shape, with ~2 mm in diameter and ~1.5 mm in length. The recovered sample was confirmed to be a single-phase garnet with an average grain size of ~3 μm by X-ray diffraction and Field-Emission Scanning Electron Microprobe (FE-SEM; JEOL-7000F) observations. We noted that the polycrystalline $Mj_{80}Py_{20}$ garnet was essentially anhydrous by the absence of OH adsorption bands in the Fourier-transform infrared spectroscopy (FTIR). The bulk density of the sample $\rho_0 = 3.521 \pm 0.021$ g cm^{-3} determined by Archimedes' method is close to the density $\rho_0 = 3.528 \pm 0.001$ g cm^{-3} calculated from the X-ray diffraction pattern, suggesting a very low porosity of the recovered sample.

Ultrasonic system in conjunction with in situ X-ray diffraction measurements

Ultrasonic measurements at simultaneous high pressures and high temperatures were conducted with a 1,500-ton Kawai-type multi-anvil apparatus (SPEED-1500) located at the beamline BL04B1 in SPring-8. The detailed information about the ultrasonic system, in situ X-ray diffraction, and X-radiography techniques has been described by Higo et al. (2008, 2009). We adopted the same 11/5 (OEL/TEL = Octahedral Edge Length of pressure medium/Truncated Edge Length of anvil) cell assemblage with that of Kono et al. (2010a) for ultrasonic and in situ X-ray diffraction measurements. A dense Al_2O_3 rod was used as a buffer rod between the sample and tungsten carbide anvil. Thin gold foils (2.5 μm in thickness) were placed on the interfaces between anvil, buffer rod, sample, and pressure marker to improve mechanical coupling. A rhenium foil tube was used as heater and an MgO window was placed in a $LaCrO_3$ sleeve for obtaining X-ray diffraction of the sample and pressure marker (Au + NaCl + BN). Temperature was measured by a $W_{97}Re_3$–$W_{75}Re_{25}$ thermocouple with the hot junction near the pressure marker.

Both ends of the polycrystalline rod sample were polished to mirror surfaces using 0.5-μm diamond powders. The travel times of ultrasonic P- and S-waves through the sample were determined by a pulse echo overlap method (Li et al. 2002, 2004; Higo et al. 2008, 2009; Kono et al. 2010a). A 10° Y-cut $LiNbO_3$ transducer, generating and receiving both compressional and transverse waves simultaneously, was bonded on the well-polished backside corner of the truncated anvil cube. Acoustic frequencies of 60 MHz for P-wave and 40 MHz for S-wave were used to determine the travel times in our study. The uncertainties of

two-way travel times are ±2 ns. The sample at simultaneous high pressures and high temperatures was monitored by X-ray radiography with a high-resolution CCD camera. The precise sample length was calculated using the calibrated image pixels (1 pixel = –2 μm, in this study) multiplied by the observed distance between the gold foils placed on the top and bottom surfaces of the sample. Uncertainties in the sample length are within ±2 μm.

In situ X-ray diffraction measurements were conducted by an energy-dispersive system with a fixed diffraction angle (6°). The unit-cell volumes of the sample and the gold pressure marker were refined by reducing full diffraction patterns following the LeBail method (Le Bail et al. 1988) with the multi-phase profile-fitting technique implemented in the EXPGUI/GSAS software package (Larson and Von Dreele 2000; Toby 2001). The experimental pressures were evaluated from the equation of state of Au (Tsuchiya 2003) from its unit-cell volume at each P–T condition.

Experimental procedures

Two in situ X-ray diffraction and ultrasonic measurements were conducted at the P–T range of 0–21 GPa and 300 ~ 2,000 K (Table 1). As shown in Fig. 1, the sample was firstly compressed to the desired pressure at room temperature and then heated to the maximum temperature to release the non-hydrostatic stress. The X-ray diffraction data, ultrasonic travel times, and sample images were then collected during the cooling process down to room temperature with 200-K temperature intervals in each cycle. In run S2888, we performed four cycles of this process up to 21 GPa and 1,300 K in the metastable field of $Mj_{80}Py_{20}$ garnet. In run S2907, the measured P–T conditions of the last cycle were up to 16 GPa and 2,000 K within the stability of $Mj_{80}Py_{20}$ garnet. When the temperature decreased from 2,000 to 1,800 K at the constant load, only X-ray diffraction data were collected without ultrasonic data due to the deterioration of the $LiNbO_3$ transducer. The samples remained as a single phase of garnet in above runs and no secondary phase was observed in the recovered samples by FE-SEM.

Experimental results

Figure 2 shows some representative in situ synchrotron X-ray diffraction patterns collected at ambient condition and high pressures and high temperatures. In all diffraction patterns, the major reflections are assigned to the garnet structure, while minor peaks are originated from the rhenium heater and gold foil in the measured cell assembly. Parise et al. (1996) and Heinemann et al. (1997) suggested that majorite containing about 20 mol % pyrope in the pyrope–majorite system adopted a tetragonal structure, although the structure for the $Mj_{80}Py_{20}$ garnet in their studies was not obvious. In our study, we could not unambiguously identify peak-splitting or appearance of new peaks as evidence for the tetragonal structure (Parise et al. 1996). This is because the energy-dispersive X-ray diffraction technique at a fixed angle bears a certain limitation in resolving the small structural distortions. Thus, we refined the cell parameters on the basis of pseudocubic structure for $Mj_{80}Py_{20}$ garnet. The zero-pressure unit-cell volume V_0 = 1,513.24 ± 0.17 Å^3 in our study agrees well with V_0 = 1,513.8 ± 1.0 Å^3 (Sinogeikin et al. 1997) and is about 0.1 % smaller than the value of 1,514.1 Å^3 (Morishima et al. 1999), which were also calculated with the cubic symmetry for $Mj_{80}Py_{20}$ garnet. The tetragonal distortion may be very small for $Mj_{80}Py_{20}$ garnet, if any, as our result is also comparable to the value of 1,513.6 ± 0.1 Å^3 reported for the same composition garnet with the tetragonal structure by Parise et al. (1996).

The unit-cell volumes of $Mj_{80}Py_{20}$ garnet at various high pressures and high temperatures are determined through in situ X-ray diffraction measurements and then fitted to the high-temperature third-order Birch–Murnaghan equation of state (HTBM; Fig. 3). The densities of $Mj_{80}Py_{20}$ garnet at various P–T conditions are determined by its molecular weight divided by the unit-cell volumes (Table 1). Fitting P–V–T data to the HTBM equation of state gives the thermoealstic parameters as follows: K_T = 160 (4) GPa, K_T' = 4.5 (5), $\partial K_T/\partial T = -0.012$ (6) GPaK^{-1}, and $\alpha = a + bT$ with values of a = 2.15 (33) × 10^{-5} K^{-1} and b = 0.43 (8) × 10^{-8} K^{-1}. As shown in Table 2, the K_T = 160 (4) GPa determined in this study is slightly higher than the value (K_T = 156 (2) GPa) derived at the fixed thermal expansion of 2.88 × 10^{-5} K^{-1} (Morishima et al. 1999), whereas the K_T' agrees well with K_T' = 4.4 (3) of their study.

Figure 4 shows the P-wave (V_P) and S-wave (V_S) velocities of $Mj_{80}Py_{20}$ garnet at various temperatures as a function of pressure. Both V_P and V_S increase almost linearly with increasing pressure, while they decrease with increasing temperature. The linear dependence on pressure and temperature of both V_P and V_S was also reported in earlier studies on grossular (Kono et al. 2010b) and pyrope (Zou et al. 2012), in contrast to the significantly nonlinear temperature dependences of V_P and V_S observed for majorite with a pyrolite minus olivine composition (Irifune et al. 2008), ringwoodite (Higo et al. 2008), and akimotoite (Zhou et al. 2013a) using the same technique. Here, we adopt the two-dimensional (*2D*) linear fitting (Li et al. 1998, 2001; Gwanmesia et al. 2006; Irifune et al. 2008; Higo et al. 2008; Kono et al. 2010b; Zou et al. 2012; Zhou et al. 2013a):

$$M = M_0 + \mathrm{d}M/\mathrm{d}P \times P + \mathrm{d}M/\mathrm{d}T \times (T-300)$$

Table 1 P–V–T, sound velocity, and elasticity data of $Mj_{80}Py_{20}$ garnet at various high pressures and high temperatures

Run. no.	P (GPa)	T (K)	V (Å^3)	Density (g/cm^3)	V_P (km/s)	V_S (km/s)	K_S (GPa)	G (GPa)
S2888								
S00	0.00 (1)	300	1,513.24 (17)	3.5279 (4)				
S07	14.64 (3)	300	1,400.76 (13)	3.8112 (3)	9.80 (2)	5.25 (1)	226.2 (12)	104.9 (3)
S13	16.20 (3)	300	1,391.58 (10)	3.8363 (3)	9.90 (3)	5.28 (1)	233.1 (10)	106.9 (4)
S20	17.06 (4)	300	1,386.63 (01)	3.8500 (1)	9.95 (2)	5.30 (2)	236.9 (10)	108.0 (7)
S27	17.77 (9)	300	1,381.38 (03)	3.8646 (1)	9.99 (3)	5.31 (1)	240.0 (18)	109.0 (4)
S06	15.00 (3)	500	1,403.55 (15)	3.8036 (4)	9.77 (3)	5.22 (2)	224.8 (20)	103.5 (2)
s12	16.63 (3)	500	1,394.44 (04)	3.8284 (1)	9.87 (3)	5.25 (2)	232.0 (17)	105.6 (5)
S19	17.35 (2)	500	1,389.38 (12)	3.8424 (3)	9.91 (3)	5.27 (1)	235.2 (20)	106.5 (2)
S26	18.10 (9)	500	1,383.61 (02)	3.8584 (1)	9.95 (3)	5.28 (1)	238.4 (19)	107.5 (3)
S04	15.44 (2)	700	1,406.07 (11)	3.7968 (2)	9.74 (3)	5.20 (2)	223.3 (14)	102.6 (6)
S11	17.09 (9)	700	1,396.75 (01)	3.8221 (1)	9.84 (3)	5.22 (1)	231.0 (15)	104.3 (5)
S18	17.81 (3)	700	1,392.10 (08)	3.8349 (2)	9.88 (3)	5.24 (1)	234.2 (18)	105.2 (3)
S25	18.66 (9)	700	1,386.90 (02)	3.8492 (1)	9.92 (3)	5.26 (1)	237.0 (20)	106.3 (2)
S03	15.87 (2)	900	1,409.40 (11)	3.7878 (3)	9.71 (3)	5.16 (1)	222.6 (18)	100.8 (3)
S10	17.52 (3)	900	1,399.55 (09)	3.8145 (2)	9.81 (3)	5.20 (2)	229.9 (15)	102.9 (6)
S17	18.26 (3)	900	1,394.49 (07)	3.8283 (2)	9.86 (3)	5.21 (1)	233.9 (17)	103.9 (4)
S24	19.02 (9)	900	1,389.96 (10)	3.8408 (2)	9.90 (2)	5.22 (1)	236.5 (10)	104.9 (4)
S02	16.52 (2)	1,100	1,411.58 (16)	3.7819 (3)	9.69 (3)	5.14 (1)	222.1 (17)	99.7 (4)
S09	17.98 (7)	1,100	1,402.31 (07)	3.8069 (2)	9.76 (3)	5.17 (1)	227.1 (17)	101.6 (4)
S16	18.74 (2)	1,100	1,396.77 (11)	3.8220 (3)	9.83 (3)	5.18 (1)	232.3 (17)	102.6 (7)
S23	19.51 (9)	1,100	1,392.52 (05)	3.8337 (1)	9.87 (3)	5.20 (2)	235.3 (12)	103.6 (4)
S15	19.41 (4)	1,300	1,399.85 (07)	3.8136 (2)	9.81 (3)	5.15 (1)	232.1 (17)	101.2 (4)
S22	19.97 (9)	1,300	1,395.16 (01)	3.8265 (1)	9.85 (3)	5.17 (1)	234.7 (17)	102.3 (4)
s2907								
s00	0.00 (1)	300	1,514.09 (17)	3.5259 (4)				
s05	17.37 (4)	300	1,385.10 (17)	3.8543 (4)	9.96 (3)	5.30 (1)	238.1 (18)	108.2 (4)
s10	18.53 (5)	300	1,375.07 (10)	3.8824 (4)	10.02 (3)	5.32 (1)	243.3 (13)	109.9 (7)
s15	19.91 (6)	300	1,370.87 (17)	3.8943 (3)	10.11 (3)	5.36 (2)	249.4 (18)	111.7 (4)
s04	17.67 (3)	500	1,388.15 (16)	3.8458 (1)	9.93 (4)	5.27 (1)	236.6 (25)	106.9 (4)
s09	18.82 (8)	500	1,380.51 (17)	3.8671 (4)	9.99 (3)	5.29 (1)	241.9 (18)	108.2 (4)
s14	20.28 (6)	500	1,373.75 (17)	3.8861 (1)	10.08 (3)	5.33 (1)	248.0 (18)	110.3 (4)
s03	18.06 (2)	700	1,391.27 (16)	3.8372 (3)	9.90 (3)	5.24 (2)	235.3 (18)	105.5 (4)
s08	19.22 (8)	700	1,383.43 (17)	3.8589 (1)	9.96 (3)	5.27 (1)	240.4 (18)	107.0 (4)
s13	20.67 (7)	700	1,376.52 (18)	3.8783 (3)	10.05 (3)	5.30 (1)	246.8 (18)	108.9 (4)
s02	18.48 (3)	900	1,393.68 (17)	3.8305 (1)	9.87 (3)	5.21 (1)	234.4 (17)	104.0 (4)
s07	19.66 (9)	900	1,386.62 (18)	3.8500 (2)	9.94 (2)	5.24 (1)	239.3 (10)	105.7 (4)
s12	21.07 (7)	900	1,376.88 (10)	3.8773 (1)	10.01 (3)	5.26 (1)	245.1 (18)	107.3 (4)
s16	16.00 (9)	2,000	1,444.86 (19)	3.6948 (3)	9.40 (3)	4.94 (2)	206.1 (11)	90.3 (7)
s17	15.25 (9)	1,800	1,443.33 (12)	3.6988 (3)				

Values in parentheses are the uncertainties in the last digit(s)

where M is V_P or V_S and dM/dP and dM/dT are their first-order pressure and temperature derivatives. A least square fitting of all the data yields: $V_P = 8.93\ (1) + 5.95\ (8) \times 10^{-2} \times P - 2.78\ (3) \times 10^{-4} \times (T - 300)$ and $V_S = 4.93\ (1) + 2.14\ (4) \times 10^{-2} \times P - 1.90\ (2) \times 10^{-4} \times (T - 300)$, respectively. The derived $V_P = 8.93$ (1) km/s of $Mj_{80}Py_{20}$ garnet at ambient condition is slightly higher than the result ($V_P = 8.82$ (1) km/s) for the majoritic garnet with the same composition using Brillouin scattering method (Sinogeikin et al. 1997), while the present $V_S = 4.93$ (1) km/s at ambient condition agrees well with $V_S = 4.91$ (2) km/s in their study.

The adiabatic bulk (K_S) and shear (G) moduli of $Mj_{80}Py_{20}$ garnet at high pressures and high temperatures

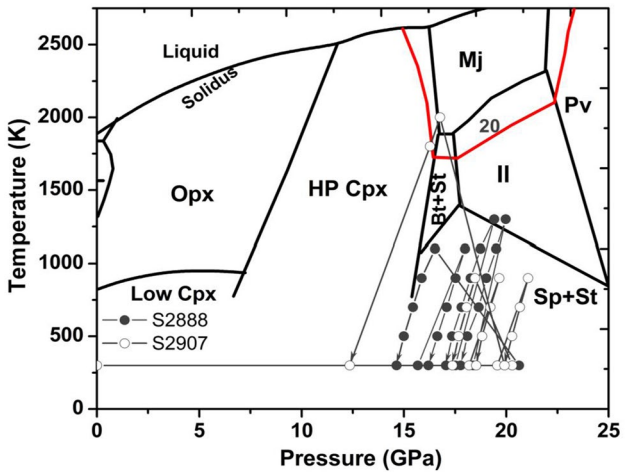

Fig. 1 Experimental pressure and temperature paths for ultrasonic and X-ray diffraction measurements on the polycrystalline $Mj_{80}Py_{20}$ garnet plotted on the phase diagram for $MgSiO_3$ (Gasparik 1990). The phase boundaries in *red lines* are stability field of $Mj_{80}Py_{20}$ garnet (Gasparik 1992). The *arrows* indicate the *P–T* paths for these measurements. *Opx* orthopyroxene, *Cpx* clinopyroxene, *HP-Cpx* high-pressure clinopyroxene, β wadsleyite, γ ringwoodite, *St* stishovite, *Mj* majorite, *II* ilmenite, *Pv* perovskite

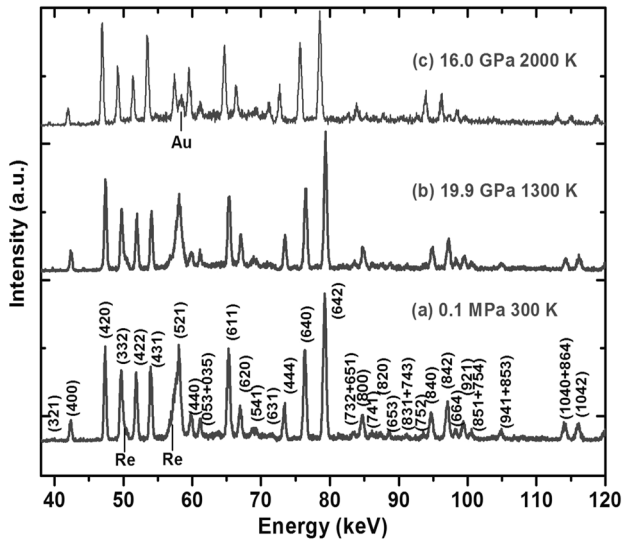

Fig. 2 Some examples of in situ X-ray diffraction patterns of $Mj_{80}Py_{20}$ garnet at **a** ambient condition (S2888), **b** 19.9 GPa, 1,300 K (S2888), and **c** 16.0 GPa, 2,000 K (S2907). The diffraction peaks from rhenium heater and gold foil are indicated by *short lines*

are determined using the data in Table 1 and the relations $K_S = \rho(V_p^2 - 4V_S^2/3)$ and $G = \rho V_S^2$. Figure 5 shows the variations of adiabatic bulk and shear moduli of $Mj_{80}Py_{20}$ garnet as a function of pressure and temperature. The data of adiabatic bulk and shear moduli are also fitted with the *2D* linear fitting method, yielding: $K_S = 161.5\ (7) + 4.42$

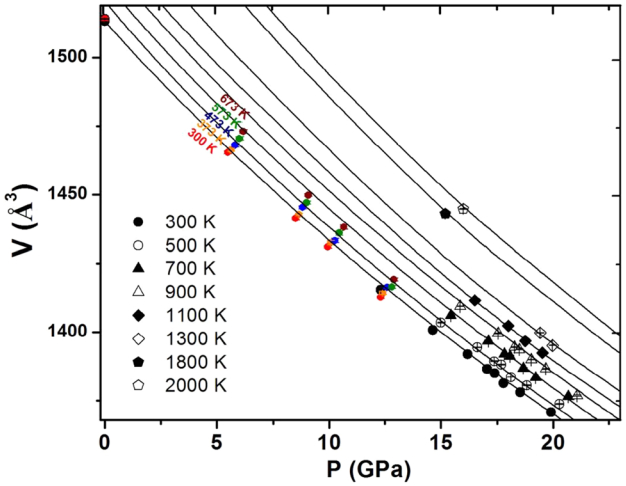

Fig. 3 P–V–T data of $Mj_{80}Py_{20}$ garnet with calculated isothermal compression curves. The *solid curves* are calculated from thermoelastic parameters derived from high-temperature third-order Birch–Murnaghan equation of state. The *color solid circles* are from one experiment result of $Mj_{80}Py_{20}$ garnet at 0~12.9 GPa (Morishima et al. 1999)

$(4) \times P - 1.54\ (2) \times 10^{-2} \times (T - 300)$ and $G = 86.2\ (2) + 1.28(1) \times P - 0.96\ (5) \times 10^{-2} \times (T - 300)$. The present bulk modulus and shear modulus at ambient condition are consistent with the results of Sinogeikin et al. (1997) within the uncertainties, while our results are lower by 2.5 and 3 % than those of Gwanmesia et al. (2000). The thermoelastic parameters of $Mj_{80}Py_{20}$ garnet in the present study are also obtained by fitting to the functions of Eulerian strain to third order (Davis and Dziewonski 1975; Gwanmesia et al. 2006, 2009, 2013). The derived elastic properties are as follows: $K_S = 158 \pm 5$ GPa, $K_S' = 4.7 \pm 0.5$, $\partial K_S/\partial T = -0.015 \pm 0.003$ GPa/K, $G = 84 \pm 3$ GPa, $G' = 1.24 \pm 0.17$, and $\partial G/\partial T = -0.011 \pm 0.001$ GPa/K. All the values derived from the linear fitting are within uncertainties of results obtained by the finite-strain fitting method.

Discussion

The elastic properties of $Mj_{80}Py_{20}$ garnet obtained in this study and previous studies on the solid solutions in the majorite–pyrope system are summarized in Table 2. At ambient conditions, the differences of elastic moduli of the garnets with various compositions in the majorite–pyrope system are relatively small. Sinogeikin et al. (1997), based on earlier studies (Yeganeh-Haeri et al. 1990; Bass and Kanzaki 1990; Yagi et al. 1992; Pacalo and Weidner 1997), proposed two models for the dependence of elastic moduli on the majorite content in this system: (1) a small linear decrease in K_S and G from Py_{100} to Mj_{100}; (2) constant

Table 2 Elastic properties of majoritic garnets along the majorite–pyrope system

Mj_xPy_{1-x} (x: mol %)	K_S (GPa)	G(GPa)	$\partial K_S/\partial P$	$\partial G/\partial P$	$\partial K_S/\partial T$ (10^{-2} GPa/K)	$\partial G/\partial T$ (10^{-2} GPa/K)	P/T conditions	References
Ultrasonic interferometry								
$Mj_{80}Py_{20}$	161.5 (7)	86.2 (2)	4.42 (4)	1.28 (1)	−1.54 (2)	−0.96 (5)	21 GPa, 2,000 K	This study
$Mj_{50}Py_{50}$	170 (5)	89 (1)	6.4 (5)	2.1 (2)	–	–	9 GPa	Liu et al. (2000)
$Mj_{50}Py_{50}$	169 (1)	90.6 (2)	5.29 (4)	1.49 (2)	−1.46 (4)	−0.933 (2)	8 GPa, 1,000 K	Gwanmesia et al. (2009)
$Mj_{40}Py_{60}$	172 (2)	91 (1)	5.34 (5)	1.53 (3)	−1.46 (4)	−0.94 (4)	8 GPa, 1,000 K	Gwanmesia et al. (2009)
$Mj_{38}Py_{62}$	171 (5)	90 (1)	6.2 (5)	1.9 (2)	–	–	9 GPa	Liu et al. (2000)
Py_{100}	170.0 (2)	93.2 (1)	4.51 (3)	1.51 (2)	−1.70 (1)	−1.07 (1)	20 GPa, 1,700 K	Zou et al. (2012)
Brillouin scattering								
Mj_{100}	166 (3)	85 (2)	4.2 (3)	1.4 (2)	–	–	15.1 GPa	Sinogeikin and Bass (2002a)
$Mj_{80}Py_{20}$	163 (3)	88 (2)	–	–	−1.43 (20)	−0.83 (10)	1,073 K	Sinogeikin and Bass (2002b)
$Mj_{50}Py_{50}$	167 (3)	90 (2)	–	–	−1.45 (20)	−0.82 (10)	1,073 K	Sinogeikin and Bass (2002b)
$Mj_{50}Py_{50}$	167 (3)	90 (2)	4.2 (4)	1.4 (2)	–	–	12.8 GPa	Sinogeikin and Bass (2002a)
Py_{100}	171 (2)	94 (2)	–	–	−1.4 (2)	−0.92 (10)	1,073 K	Sinogeikin and Bass (2002b)
Isothermal static compression								
$Mj_{80}Py_{20}$	160 (4)	–	4.5 (5)	–	−1.2 (6)	–	23 GPa, 773 K	This study
$Mj_{80}Py_{20}$	156 (2)	–	4.4 (3)	–	−1.9 (3)	–	23 GPa, 773 K	Morishima et al. (1999)
$Mj_{38}Py_{62}$	160 (3)	–	4.9 (5)	–	−1.9 (4)	–	11 GPa, 1,163 K	Wang et al. (1998)

K_S and G from Mj_{100} to $Mj_{70}Py_{30}$, followed by a step-like decrease at $Mj_{70}Py_{30}$–$Mj_{80}Py_{20}$ and a gradual increase to Mj_{100}. As shown in Fig. 6, our results are rather compatible with the model (2), although we cannot rule out the possibility of the linear dependence (Pacalo and Weidner 1997; Gwanmesia et al. 2000). The different synthesis conditions, quench history, and measured methods make it difficult to describe the scattering nature of the elastic moduli data on the majoritic garnets along the majorite–pyrope system, especially the compositional dependency of elastic moduli in this system. It is also unclear whether the cubic-tetragonal symmetry transformation at $Mj_{75}Py_{25}$ (Parise et al. 1996) affects the elastic moduli of majoritic garnets in this system. Further systematic studies are required to clarify this issue, although the effects of this phase transformation seem not to be very significant (Sinogeikin et al. 1997).

The newly obtained pressure derivatives of the adiabatic bulk modulus $K_S' = (\partial K_S/\partial P)_T$ and the shear modulus $G' = (\partial G/\partial P)_T$ of $Mj_{80}Py_{20}$ garnet are 4.42 (4) and 1.28 (1), respectively, which are nearly identical with the results of Py_{100} [$K_S' = 4.51$ (3), $G' = 1.51$ (2); Zou et al. 2012] and slightly lower than those of $Mj_{50}Py_{50}$ and $Mi_{40}Py_{60}$ ($Mj_{50}Py_{50}$: $K_S' = 5.29$ (4), $G' = 1.49$ (2); $Mj_{40}Py_{60}$: $K_S' = 5.34$ (5), $G' = 1.53$ (3); Gwanmesia et al. 2009) using the similar experimental methods. Furthermore, the pressure derivatives of elastic moduli for $Mj_{80}Py_{20}$ garnet in the present study are in good agreement with those of Mj_{100} and $Mj_{50}Py_{50}$ determined by Brillouin scattering techniques (Sinogeikin and Bass 2002a). On the other hand, our data are contradictory to the large pressure derivatives for $Mj_{50}Py_{50}$ ($K' = 6.4$, $G' = 2.1$) and $Mj_{38}Py_{62}$ ($K' = 6.2$, $G' = 1.9$) reported by Liu et al. (2000). Their high-pressure derivatives may be caused by the non-hydrostatic stresses on the cell assembly without heating at high pressures (Gwanmesia et al. 2006). It should also be noted that the K_T' of $Mj_{80}Py_{20}$ garnet determined in this study is also compatible with those derived from the isothermal static compression of $Mj_{80}Py_{20}$ (Morishima et al. 1999) and $Mj_{38}Py_{62}$ (Wang et al. 1998). Thus, we conclude that the pressure derivatives of elastic moduli are not sensitive to the majorite content in the majorite–pyrope system, in contrast to the results by Liu et al. (2000).

The temperature derivatives of the elastic moduli for $Mj_{80}Py_{20}$ garnet and other majorite–pyrope solid solutions are listed in Table 2. The values of $(\partial K_S/\partial T)_P = -1.54$ (2) $\times 10^{-2}$ GPa/K and $(\partial G/\partial T)_P = -0.96$ (5) $\times 10^{-2}$ GPa/K of $Mj_{80}Py_{20}$ garnet in this study are in agreement with those derived from Brillouin scattering measurements on the same composition and also comparable to those of $Mj_{50}Py_{50}$ and Py_{100} garnets (Sinogeikin and Bass 2002b). Moreover, our results are also essentially identical with those of $Mj_{50}Py_{50}$ and $Mj_{40}Py_{60}$ garnets using the similar experimental method by Gwanmesia et al. (2009). When compared with the results of Py_{100} (Zou et al. 2012), our results are higher by about 10 and 11 %, respectively. The temperature derivatives of elastic moduli of $Mj_{80}Py_{20}$ garnet in this study are close to those of other majoritic garnets in the majorite–pyrope system, indicating that temperature derivatives of elastic moduli are insensitive to the majorite content in this system, as proposed by Wang et al. (1998)

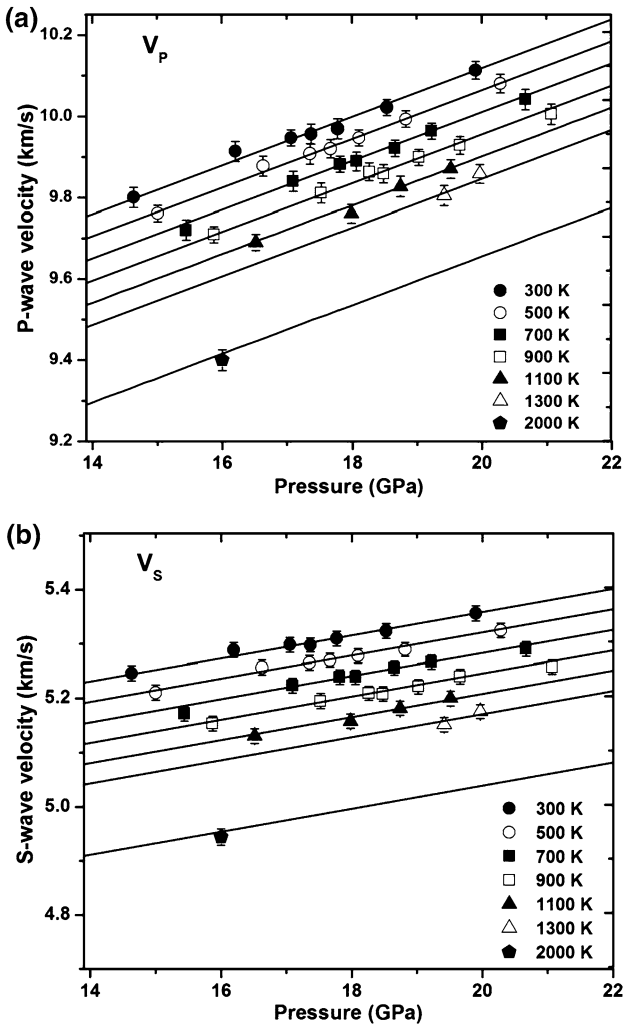

Fig. 4 P (**a**) and S (**b**) wave velocities of $Mj_{80}Py_{20}$ garnet at high pressures and high temperatures. The *solid lines* represent the two-dimensional linear fitting curves. *Error bars* indicate the uncertainties of velocities

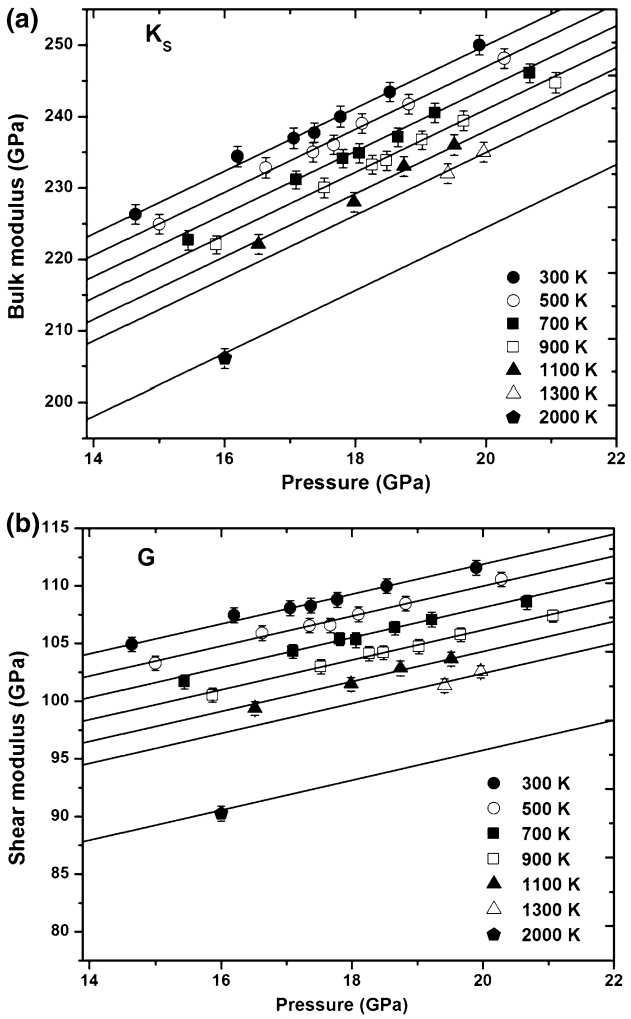

Fig. 5 Adiabatic Bulk (**a**) and shear (**b**) moduli of $Mj_{80}Py_{20}$ garnet at high pressures and high temperatures. The *solid lines* represent the two-dimensional linear fitting curves. *Error bars* indicate the uncertainties of elastic moduli

from the isothermal static measurement on $Mj_{38}Py_{62}$ and Py_{100} garnets.

The temperature dependences in elastic velocities of mantle minerals are important to constrain the velocity profile and mineralogy of the mantle transition zone. In Fig. 7, the V_P and V_S of $Mj_{80}Py_{20}$ garnet calculated from current experimental data decrease linearly with the increasing temperature at the selected pressures of 16, 18, and 20 GPa, although a nonlinear behavior in the majorite with a pyrolite minus olivine composition was reported by Irifune et al. (2008). The discrepancy may be explained by the difference in the mineral composition (Zou et al. 2012) and the limitation of the measured temperatures range in elastic velocity study (Zhou et al. 2013a). Further studies on other minerals at higher temperatures are needed to clarify this issue.

In Fig. 8, we evaluate the sound velocity profiles of $Mj_{80}Py_{20}$ garnet and other solid solutions in the majorite–pyrope system (pyrope, Zou et al. 2012; $Mg_4Si_4O_{12}$ majorite, Zhou et al. 2013b) along a typical adiabatic geotherm in the mantle transition zone (Brown and Shankland 1981). The present Al-bearing majoritic garnet ($Mj_{80}Py_{20}$) produces slightly higher velocities than the $Mg_4Si_4O_{12}$ majorite, while lower than those of pyrope and the typical seismological models. Therefore, petrological model with the majorite-rich garnet (e.g., pyrolite,MORB or eclogite) would produce lower velocities than PREM/AK135 in the mantle transition zone, especially for the lower part of this region (Irifune et al. 2008; Kono et al. 2012).

The majoritic garnet is a dominated phase in the mantle transition zone (Ringwood and Major 1971; Akaogi and Akimoto 1977; Irifune and Ringwood 1987). The study

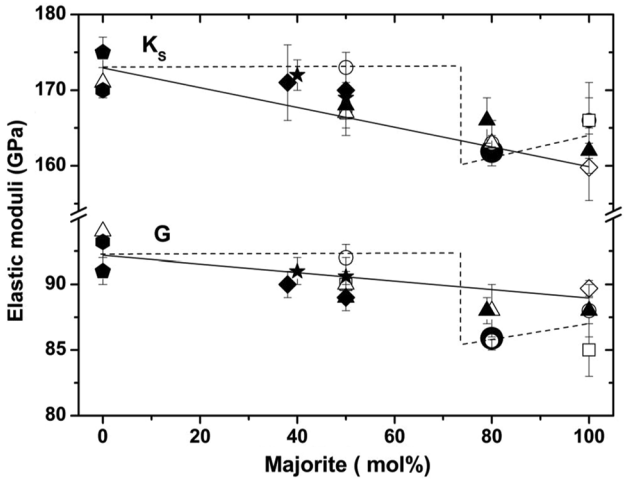

Fig. 6 Ambient elastic moduli (K_S and G) as a function of the majorite composition in the majorite–pyrope system. *Open* and *solid symbols* represent those measured with Brillouin scattering and ultrasonic techniques, respectively. The *open diamond*, *circle*, *triangle* and *square symbols* are from Pacalo and Weidner (1997) and Sinogeikin et al. (1997), Sinogeikin and Bass (2002a, b), while the large solid circle, triangle, diamond, pentagon, star, and hexagon symbols are from this study, Gwanmesia et al. (2000), Liu et al. (2000), Gwanmesia et al. (2006), Gwanmesia et al. (2009), and Zou et al. (2012). The dashed and solid lines represent the compositional dependence proposed by Sinogeikin et al. (1997)

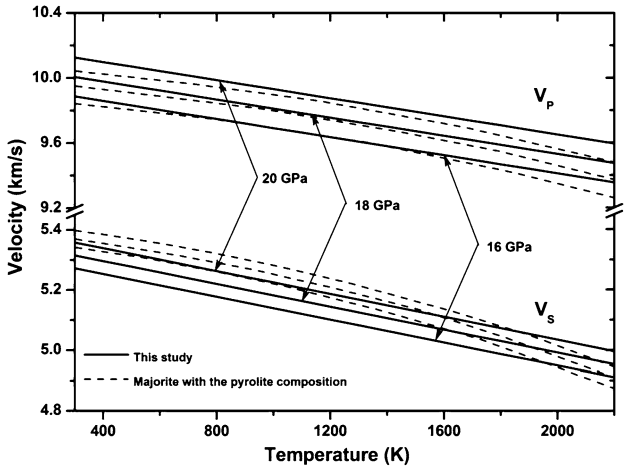

Fig. 7 Variations of sound velocities of $Mj_{80}Py_{20}$ garnet as a function of temperature at selected pressures in the mantle transition zone region. The *solid curves* show the P- and S-wave velocities (V_P and V_S) derived from the present study. The *dashed curves* represent those from the sound velocity measurements on the majorite with the pyrolite composition (Irifune et al. 2008)

of elastic properties of majoritic garnet will thus contribute significantly to modeling the sound velocity profile of the mantle transition zone. For example, the high velocity gradients in the mantle transition zone at depths of 410–520 km have been attributed to the gradual dissolution of

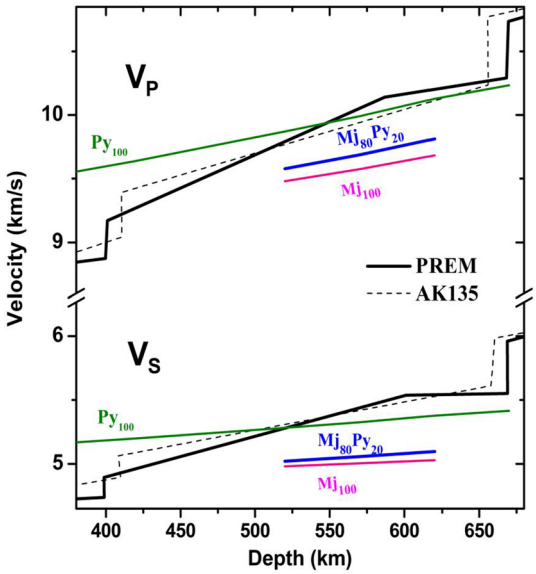

Fig. 8 Comparison of velocities of the majoritic garnets in the majorite–pyrope system along a typical adiabatic mantle geotherm in mantle transition zone (Brown and Shankland 1981). *Black solid* and *dashed lines* show the velocity profiles from seismic models of PREM (Dziewonski and Anderson 1981) and AK135 (Kennett and Engdahl 1991). *Blue*, *pink*, and *olivine solid lines* are calculated from the velocity data of $Mj_{80}Py_{20}$ (this study), majorite (Mj_{100}, Zhou et al. 2013b), and pyrope (Py_{100}, Zou et al. 2012)

the clinopyroxene into the majoritic garnet with increasing depth (Bass and Anderson 1984; Irifune and Ringwood 1987; Irifune and Isshiki 1998; Sinogeikin and Bass 2002a), while a recent study based on sound velocity measurements on the majoritic garnet with a pyrolite minus olivine composition suggested a smaller velocity gradient for the mantle transition zone (Irifune et al. 2008). Therefore, we evaluate the velocity gradient $\partial V_S/\partial Z$ of $Mj_{80}Py_{20}$ garnet [~0.7 (m/s)/km, this study], $Mg_4Si_4O_{12}$ majorite [~0.4 (m/s)/km, Zhou et al. 2013b] and pyrope [~0.8 (m/s)/km, Zou et al. 2012], which are 3–6 times lower than the observed velocity gradients of PREM/AK135 [2.1–2.6 (m/s)/km, Dziewonski and Anderson 1981; Kennett and Engdahl 1991] in the mantle transition zone. The majoritic garnets in the majorite–pyrope system do not yield steep velocity slopes to account for the large velocity gradient in the mantle transition zone. Moreover, the velocity slope of the ~5 wt% iron-bearing majorite [~0.591 (m/s)/km; Murakami et al. 2008] is comparable to that of the majorite–pyrope system. It has also been suggested that the gradual formation of $CaSiO_3$ perovskite from the majoritic garnet in a pyrolite minus olivine composition or the presence of chemical heterogeneity may account for the steep slope of seismic velocity in the deeper regions of the mantle transition zone (Irifune et al. 2008). Further studies about the effect of chemical composition such as calcium and sodium

impurities, as well as that of the lithology of the mantle transition zone on the seismic velocities, are needed to constrain the mineralogical model of this region in the Earth's mantle.

Acknowledgments The authors are grateful to H. Ohfuji and M. Nishi for their helps in FE-SEM observations. We thank C. Zhou, T. Kunimoto, Y. Tange, N. Cai, W. Du, and X. Wang for their experimental technical assistances and valuable discussions. We appreciate Y. Nishihara for his help in FTIR measurements. We are also grateful for constructive reviews by Dr. C. McCammon and two anonymous reviewers. The present study is supported by the Grant-in-Aid for Scientific Research (S) by JSPS to T. Irifune (Grant No. 25220712).

References

Akaogi M, Akimoto S (1977) Pyroxene-garnet solid solution equilibria in the systems $Mg_4Si_4O_{12}$-$Mg_3Al_2Si_3O_{12}$ and at high pressures and temperatures. Phys Earth Planet Inter 15:90–106

Akaogi M, Tanaka A, Ito E (2002) Garnet–ilmenite–perovskite transitions in the system $Mg_4Si_4O_{12}$-$Mg_3Al_2Si_3O_{12}$ at high pressures and high temperatures: phase equilibria, calorimetry and implications for mantle structure. Phys Earth Planet Inter 132:303–324

Bass JD, Anderson DL (1984) Composition of the upper mantle: geophysical tests of two petrological models. Geophys Rev Lett 11:237–240

Bass DJ, Kanzaki M (1990) Elasticity of majorite-pyrope solid solution. Geophys Res Lett 17:1989–1992

Brown JM, Shankland TJ (1981) Thermodynamic parameters in the Earth as determined from seismic profiles. Geophys J R Astr Soc 66:579–596

Coleman LC (1977) Ringwoodite and majorite in the Catherwood meteorite. Can Mineral 15:97–101

Davis GF, Dziewonski AM (1975) Homogeneity and constitution of the Earth's lower mantle and outer core. Phys Earth Planet Inter 10:336–343

Dziewonski AM, Anderson DL (1981) Preliminary reference Earth model. Phys Earth Planet Inter 25:297–356

Gasparik T (1990) Phase relations in the transition zone. J Geophys Res 95:15751–15769

Gasparik T (1992) Melting experiments on the enstatite-pyrope join at 80–152 Kbar. J Geophys Res 97:15181–15188

Gwanmesia GD, Chen G, Liebermann RC (1998) Sound velocities in $MgSiO_3$-garnet to 8 GPa. Geophys Res Lett 25:4553–4556

Gwanmesia GD, Liu J, Chen G, Kesson S, Rigden SM, Liebermann RC (2000) Elasticity of pyrope ($Mg_3Al_2Si_3O_{12}$)—majorite ($Mg_4Si_4O_{12}$) garnet solid solution. Phys Chem Miner 27:445–452

Gwanmesia GD, Zhang J, Darling K, Kung J, Li B, Wang L, Neuville D, Liebermann RC (2006) Elasticity of Polycrystalline Pyrope ($Mg_3Al_2Si_3O_{12}$) to 9 GPa and 1000°C. Phys Earth Planet Inter 155:179–190

Gwanmesia GD, Wang L, Heady A, Liebermann RC (2009) Pressure and temperature dependence of the elasticity of pyrope-majorite [$Py_{60}Mj_{40}$ and $Py_{50}Mj_{50}$] garnets solid solution measured by ultrasonic interferometry technique. Phys Earth Planet Inter 174:105–112

Gwanmesia GD, Wang L, Heady A, Liebermann RC (2013) Elasticity and sound velocities of polycrystalline grossular garnet ($Ca_3Al_2Si_3O_{12}$) at simultaneous high pressures and high temperatures. Phys Earth Planet Inter 228:80–87

Heinemann S, Sharp TG, Seifert F, Rubie DC (1997) The cubic-tetragonal phase transition in the system majorite ($Mg_4Si_4O_{12}$)—pyrope ($Mg_3Al_2Si_3O_{12}$) and garnet symmetry in the earth's transition zone. Phys Chem Miner 24:206–221

Higo Y, Inoue T, Irifune T, Funakoshi K-I, Li B (2008) Elastic wave velocities of $(Mg_{0.91}Fe_{0.09})_2SiO_4$ ringwoodite under P-T conditions of the mantle transition region. Phys Earth Planet Inter 166:67–174

Higo Y, Kono Y, Inoue T, Irifune T, Funakoshi K-I (2009) A system for measuring elastic wave velocity under high pressure and high temperature using a combination of ultrasonic measurement and the multi-anvil apparatus at SPring-8. J Synchrotron Radia 16:762–768

Hirose K, Fei Y, Ma Y, Mao H-K (1999) The fate of subducted basaltic crust in the Earth's lower mantle. Nature 397:53–56

Irifune T, Isshiki M (1998) Iron partitioning in a pyrolite mantle and the nature of the 410-km seismic discontinuity. Nature 392:702–705

Irifune T, Ringwood AE (1987) Phase transformations in primitive MORB and pyrolite compositions to 25 GPa and some geophysical implications. In: Manghnani MH, Syono Y (eds) High pressure research in mineral physics. Terra Scientific, Tokyo, pp 231–242

Irifune T, Ringwood AE (1993) Phase transformations in subducted oceanic crust and buoyancy relationships at depths of 600–800 km in the mantle. Earth Planet Sci Lett 117:101–110

Irifune T, Sekine T, Ringwood AE, Hibberson WO (1986) The eclogite-garnetite transformation at high pressure and some geophysical implications. Earth Planet Sci Lett 77:245–256

Irifune T, Koizumi T, Ando J (1996) An experimental study of the garnet-perovskite transformation in the system $MgSiO_3$-$Mg_3Al_2Si_3O_{12}$. Phys Earth Planet Inter 96:147–157

Irifune T, Higo Y, Inoue T, Kono Y, Ohfuji H, Funakoshi K (2008) Sound velocities of majorite garnet and the composition of the mantle transition region. Nature 451:814–817

Kavner A, Sinogeikin SV, Jeanloz R, Bass JD (2000) Equation of state and strength of natural majorite. J Geophys Res 105:5963–5971

Kennett BL, Engdahl ER (1991) Traveltimes for global earthquake location and phase identification. Geophys J Int 105:429–465

Kono Y, Irifune T, Higo Y, Inoue T, Barnhoorn A (2010a) P-V–T relation of MgO derived by simultaneous elastic wave velocity and in situ X-ray measurements: a new pressure scale for the mantle transition region. Phys Earth Planet Int 183:196–211

Kono Y, Gréaux S, Higo Y, Ohfuji H, Irifune T (2010b) Pressure and temperature dependences of elastic properties of grossular garnet up to 17 GPa and 1650 K. J Earth Sci 21:782

Kono Y, Irifune T, Ohfuji H, Higo Y, Funakoshi K-I (2012) Sound velocities of MORB and absence of a basaltic layer in the mantle transition region. Geophys Res Lett 39:L24306

Kubo A, Akaogi M (2000) Post-garnet transitions in the system $Mg_4Si_4O_{12}$–$Mg_3Al_2Si_3O_{12}$ up to 28 GPa: phase relations of garnet, ilmenite and perovskite. Phys Earth Planet Int 121:85–102

Larson AC, Von Dreele RB (2000) GSAS general structure analysis system operation manual. Los Alamos Natl Lab LAUR 86–748:1–179

Le Bail A, Duroy H, Fourquet JL (1988) Ab initio structure determination of $LiSbWO_6$ by X-ray powder diffraction. Mater Res Bull 23:447–452

Li B, Liebermann RC (2007) Indoor seismology by probing the Earth's interior by using sound velocity measurements at high pressures and temperatures. Proc Natl Acad Sci USA 104:9145–9150

Li B, Jackson I, Gasparik T, Liebermann RC (1996) Elastic wave velocity measurement in multi-anvil apparatus to 10 GPa using ultrasonic interferometry. Phys Earth Planet Inter 98:79–91

Li B, Liebermann RC, Weidner DJ (1998) Elastic Moduli of Wadsleyite (β-Mg_2SiO_4) to 7 Gigapascals and 873 Kelvin. Science 281:675–676

Li B, Liebermann RC, Weidner DJ (2001) P-V-V_P-V_S-T measurements on wadsleyite to 7 GPa and 873 K: implications for the 410-km seismic discontinuity. J Geophys Res 106:30575–30591

Li B, Chen K, Kung J, Liebermann RC, Weidner DJ (2002) Ultrasonic measurement using transfer function method. J Phys Cond Matter 14:11337–11342

Li B, Kung J, Liebermann RC (2004) Modern techniques in measuring elasticity of Earth materials at high pressure and high temperature using ultrasonic interferometry in conjunction with synchrotron X-radiation in multi-anvil apparatus. Phys Earth Planet Int 143–144:559–574

Liu J, Chen G, Gwanmesia G, Liebermann RC (2000) Elastic wave velocities of pyrope–majorite garnets ($Py_{62}Mj_{38}$ and $Py_{50}Mj_{50}$) to 9 GPa. Phys Earth Planet Int 120:153–163

Mao H-K, Bell PM, Boctor NZ (1982) The mineral chemistry of majorite in L6 chondrites. Carnegie Inst Washington Year b 81:279–281

Meyer HOA (1987) Inclusions in diamond. In: Nixon PH (ed) Mantle Xenoliths. JohnWiley & Sons Ltd, Chichester, pp 501–522

Moore RO, Gurney JJ (1985) Pyroxene solid solution in garnets included in diamond. Nature 318:553–555

Morishima H, Ohtani E, Kato T, Kubo T, Suzuki A, Kikegawa T, Shimomura O (1999) The high-pressure and temperature equation of state of a majorite solid solution in the system of $Mg_4Si_4O_{12}$-$Mg_3Al_2Si_3O_{12}$. Phys Chem Mineral 27:3–10

Murakami M, Sinogeikin SV, Litasov K, Ohtani E, Bass JD (2008) Single-crystal elasticity of iron-bearing majorite to 26 GPa: implications for seismic velocity structure of the mantle transition zone. Earth Planet Sci Lett 274:339–345

Ono S, Ito E, Katsura T (2001) Mineralogy of subducted basaltic crust (MORB) from 25 to 37 GPa, and chemical heterogeneity of the lower mantle. Earth Planet Sci Lett 190:57–63

Pacalo REG, Weidner DJ (1997) Elasticity of majorite, $MgSiO_3$ tetragonal garnet. Phys Earth Planet Int 99:145–154

Parise JB, Wang Y, Gwanmesia GD, Zhang J, Sinelnikov Y, Chmielowski J, Weidner DJ, Liebermann RC (1996) The symmetry of garnets on the pyrope ($Mg_3Al_2Si_3O_{12}$)—majorite ($MgSiO_3$) join. Geophys Res Lett 23:3799–3802

Rigden SM, Gwanmesia GD, Liebermann RC (1994) Elastic wave velocities of a pyrope-majorite garnet to 3 GPa. Phys Earth Planet Int 86:35–44

Ringwood AE, Major A (1971) Synthesis of majorite and other high pressure garnets and perovskites. Earth Planet Sci Lett 12:411–418

Sinogeikin SV, Bass JD (2002a) Elasticity of Majorite and Majorite-Pyrope solid solution to high pressure: Implicaitions for the Transition Zone. Geophys Res Lett 29:2453–2456

Sinogeikin SV, Bass JD (2002b) Elasticity of pyrope and majorite-pyrope solid solutions to high temperatures. Earth Planet Sci Lett 203:549–555

Sinogeikin SV, Bass JD, O'Neill B, Gasparik T (1997) Elasticity of tetragonal end-member majorite and solid solution in the system $Mg_4Si_4O_{12}$-$Mg_3Al_2Si_3O_{12}$. Phys Chem Miner 24:115–121

Toby BH (2001) EXPGUI, a graphical user interface for GSAS. J Appl Crystallogr 34:210–213

Tsuchiya T (2003) First-principles prediction of the P–V–T equation of state of gold and the 660-km discontinuity in Earth's mantle. J Geophys Res 108(B10):2462

Wang Y, Weidner DJ, Zhang J, Gwanmesia GD, Liebermann RC (1998) Thermal equation of state of garnets along the pyrope-majorite join. Phys Earth Planet Int 105:59–71

Yagi T, Uchiyama Y, Akaogi M, Ito E (1992) Isothermal compression of $MgSiO_3$ tetragonal garnet. Phys Earth Planet Int 74:1–7

Yeganeh-Haeri A, Weidner DJ, Ito E (1990) Elastic properties of the pyrope-majorite solid solution series. Geophys Res Lett 17:2453–2456

Zhou C, Gréaux S, Nishiyama N, Irifune T, Higo Y (2013a) Sound velocities measurement on $MgSiO_3$ akimotoite at high pressures and high temperatures with simultaneous in situ X-ray diffraction and ultrasonic study. Phys Earth Planet Int 228:97–105

Zhou C, Gréaux S, Nishiyama N, Irifune T, Higo Y (2013b) Sound velocities measurement on $MgSiO_3$ akimotoite at high pressures and high temperatures with simultaneous in situ X-ray diffraction and ultrasonic study. Phys Earth Planet Int 228:97–105, Reference therein

Zou Y, Irifune T, Gréaux S, Whitaker ML, Shinmei T, Ohfuji H, Negishi R, Higo Y (2012) Elasticity and sound velocities of polycrystalline $Mg_3Al_2(SiO_4)_3$ garnet up to 20 GPa and 1700 K. J Appl Phys 112:014910